JACS
JOURNAL OF THE AMERICAN CHEMICAL SOCIETY
Article
pubs.acs.org/JACS

Persistent Organic Nanopores Amenable to Structural and Functional Tuning

Xiaoxi Wei,[†,¶,‡] Guoqing Zhang,[†,‡] Yi Shen,[∥,‡] Yulong Zhong,[†] Rui Liu,[†,¶] Na Yang,[†] Fayez Y. Al-mkhaizim,[¶] Mark A. Kline,[¶] Lan He,[§] Minfeng Li,[†] Zhong-Lin Lu,[*,†] Zhifeng Shao,[*,∥] and Bing Gong[*,¶,†]

[†]College of Chemistry, Beijing Normal University, Beijing 100875, China
[¶]Department of Chemistry, The State University of New York at Buffalo, Buffalo, New York 14260, United States
[∥]Bio-ID Center, School of Biomedical Engineering, Shanghai Jiao Tong University, Shanghai 200240, China
[§]National Institute for Food and Drug Control, Beijing 100050, China

Supporting Information

ABSTRACT: Rigid macrocycles **2**, which share a hybrid backbone and the same set of side chains while having inner cavities with different inward-pointing functional groups, undergo similar nanotubular assembly as indicated by multiple techniques including ^{1}H NMR, fluorescence spectroscopy, and atomic force microscopy. The formation of tubular assemblies containing subnanometer pores is also attested by the different transmembrane ion-transport behavior observed for these macrocycles. Vesicle-based stopped-flow kinetic assay and single-channel electrophysiology with planar lipid bilayers show that the presence of an inward-pointing functional (**X**) group in the inner cavity of a macrocyclic building block exerts a major influence on the transmembrane ion-transporting preference of the corresponding self-assembling pore. Self-assembling pores with inward-pointing amino and methyl groups possess the surprising and remarkable capability of rejecting protons but are conducive to transporting larger ions. The inward-pointing groups also resulted in transmembrane pores with a different extent of positive electrostatic potentials, leading to channels having different preferences for transporting chloride ion. Results from this work demonstrate that synthetic modification at the molecular level can profoundly impact the property of otherwise structurally persistent supramolecular assemblies, with both expected tunability and suprisingly unusual behavior.

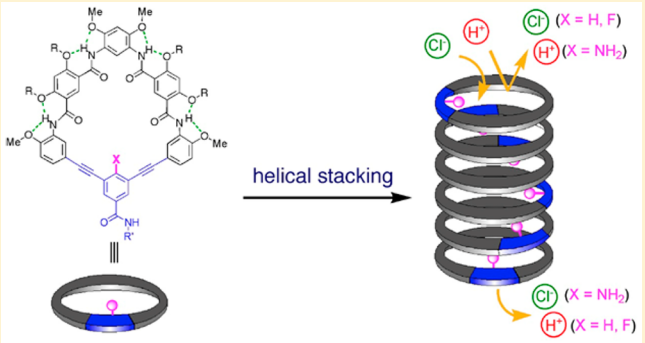

INTRODUCTION

Void-containing molecular and supramolecular structures,[1,2] especially those with small (≤2 nm) and sub-nm pores of a defined size,[4−7] provide confinement under which many fascinating phenomena have been predicted or observed. Among known systems,[2,3] the stacking of ring-like molecules leads to tubular assemblies that can be modified by varying the constituent molecular components.[3,4] Of particular interest is the stacking of rigid macrocycles, which leads to nanotubes containing nondeformable inner pores with precisely defined diameters. Such self-assembling nanopores, if amenable to structural modifications, may afford systems with novel molecular recognitions, mass transport, and many other capabilities.

Since their discovery[8a] and the elucidation of the mechanism of their formation,[8b] aromatic oligoamide macrocycles **1** (Figure 1) have served as the basis for creating several classes of rigid macrocycles[9] that have greatly expanded the inventory of such shape-persistent molecular objects.[8−13] The stacking of **1**[14] along with the discrete[15] or extremely strong[16] tubular assembly of derivatives of **1** have demonstrated the persistent assembly of these macrocycles.

The tubular assemblies of **1** have prompted us to probe their functions, one of which involves ion transport across membranes. Our effort had uncovered cation-selective channels with very high conductance.[17]

Although the inner pores of stacked **1** appear to offer a prototype based on which different synthetic channels[18] might be developed, unfortunately, tuning the inner pore is not feasible since the cavity of **1** contains few positions that would allow structural alterations without compromising the integrity of the H-bond-constrained[19] macrocyclic backbone.

We report herein the formation of nanotubular stacks of macrocycles **2** (Figure 1) and their ion-transport properties. The inner pores of the tubular stacks, structurally modified by incorporating macrocycles sharing the same periphery but

Received: December 4, 2015
Published: February 13, 2016

DOI: 10.1021/jacs.5b12698
J. Am. Chem. Soc. 2016, 138, 2749−2754

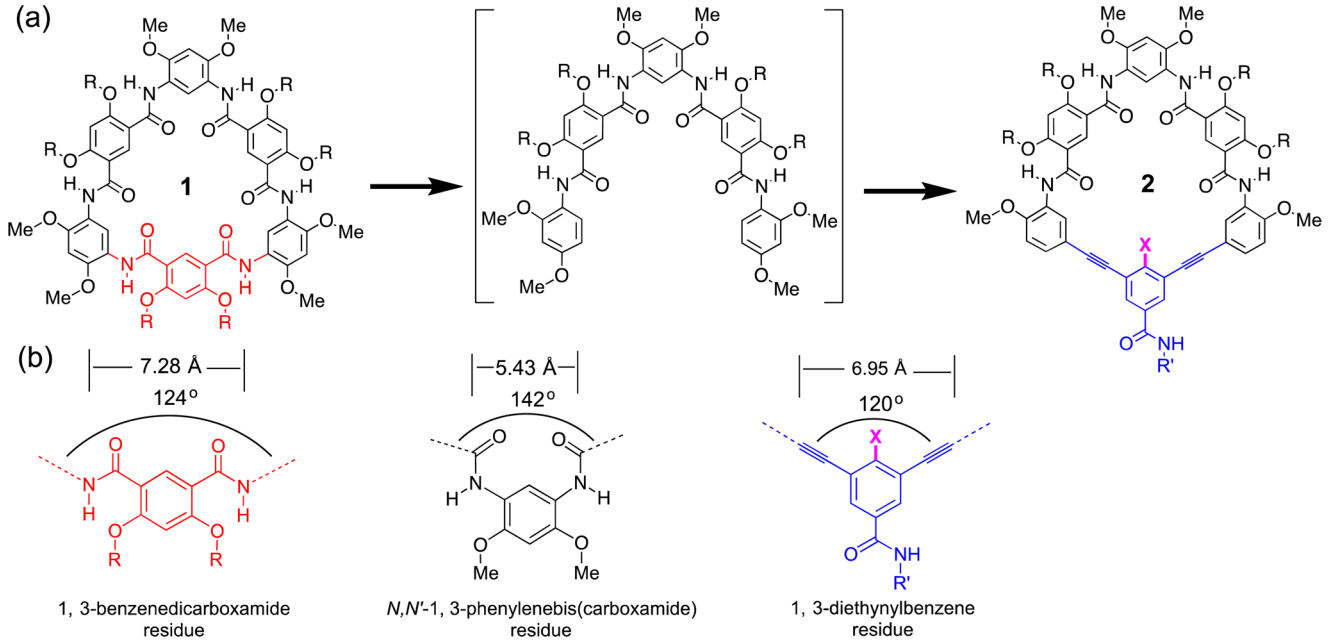

Figure 1. (a) Design of macrocycle **2** by integrating the backbone of **1** and that of *m*-PE macrocycles. (b) Comparison of the two different monomeric residues of **1** with 1, 3-diethynylbenzene residue.

having cavities with inward-pointing functional groups, were found to exhibit different ion-transporting preferences.

Macrocycles **2** can be regarded as being derived from merging the backbones of **1** and oligo(*m*-phenylene ethynylene) (or *m*-PE) macrocycles, another class of well-studied rigid macrocycles.[10] Thus, replacing part (~1/3), i.e., a 1,3-benzenedicarboxamido residue, of **1** with a diethynylbenzene unit (Figure 1a) results in a hybrid backbone containing a segment that allows inward-pointing functional groups (**X**) to be placed. Results based on simple modeling indicate that the introduced diethynylbenzene moiety (Figure 1b, blue) closely matches the shape of the replaced residue (Figure 1b, red). With their overall flat shape (Figure S41), macrocycles **2** are expected to aggregate anisotropically,[16] i.e., to stack into tubular assemblies. A secondary amide side chain is included in **2** to reinforce the directionality of the stacking and to also facilitate the characterization of the supramolecular assemblies.

Scheme 1. Synthesis of Macrocycles 2

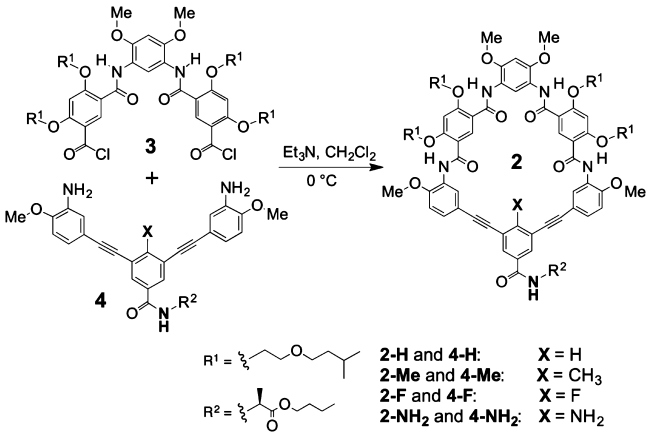

RESULTS AND DISCUSSION

Synthesis. The synthesis of macrocycles **2** involves coupling trimer diacid chloride **3** with the corresponding trimer diamines **4** (Scheme 1).[20] Thus, a mixture of **3**, prepared from the corresponding diacid (0.37 mmol), and **4-H** (0.304 mmol) in CH_2Cl_2 was stirred at 0 °C for 3 h. The reaction mixture was then washed with water, saturated brine, and dried over anhydrous Na_2SO_4. Removing CH_2Cl_2 led to a residue that was purified by column chromatography (silica gel), giving **2-H** as a white solid (185 mg, 41%). Macrocycles **2-Me**, **2-F**, and **2-NH$_2$** were prepared under the same conditions, with unoptimized yields ranging from 11% to 24% after extensive purification (see Supporting Information).

Macrocycles 2 Undergo Anisotropic Aggregation in Nonpolar Solvents. In $CDCl_3$, the ^{1}H NMR signals of **2-H** are considerably broadened, which indicates that the molecules of **2-H** undergo decreased molecular motion due to aggregation; in DMSO-d_6, the spectrum of **2-H** contains well-dispersed peaks, suggesting that the individual molecules were fully solvated (Figures S23 and S24). Similarly, the ^{1}H NMR spectra of **2-Me**, **2-F**, and **2-NH$_2$** contain signals that are broadened in $CDCl_3$ but are well-resolved in DMSO-d_6 (Figures S25–S30), indicating that, in $CDCl_3$, these macrocycles undergo aggregation that is interrupted in the much more polar DMSO.

In comparison to their noncyclic precursors (Figure S31), macrocycles **2** exhibit much stronger absorption and emission, which allows their aggregation to be examined at significantly reduced concentrations (1–5 μM). In DMF in which **2-H** is fully solvated, an emission band at 385 nm is observed; in $CCl_4/CHCl_3$ (7/3, v/v), a broad band at 455 nm, which can be attributed to π-stacked aromatic rings[21a] that exist in the ground state and give "excimer-like" emissions, appears (Figure 2a).[21b] Consistent with ground-state association, monitoring the emission of **2-H** at 385 and 455 nm reveals two bands around 300 and 280 nm, respectively, in the excitation spectra (Figure 2b). The excitation band at 280 nm, being monitored at 455 nm which corresponds to the aggregated state of **2-H**, is blue-shifted relative to the 300 nm excitation band due to the

DOI: 10.1021/jacs.5b12698
J. Am. Chem. Soc. 2016, 138, 2749–2754

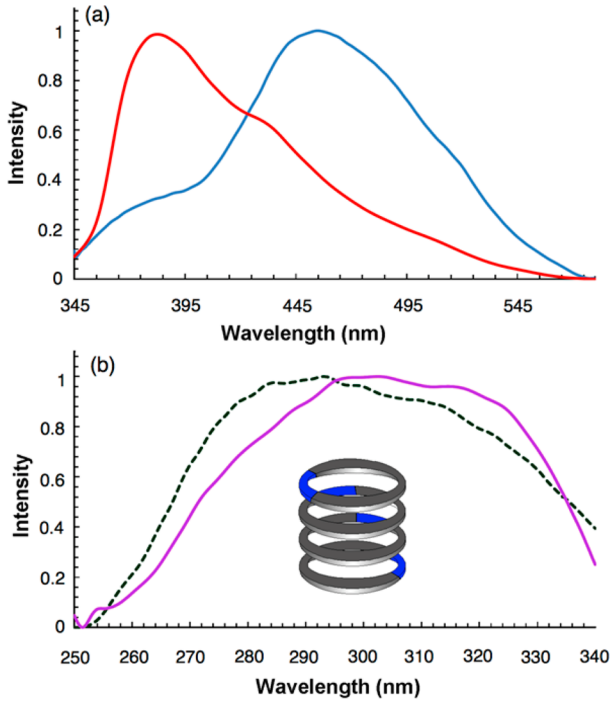

Figure 2. (a) Normalized emission spectra of **2-H** (1 μM) in DMF (red) and $CCl_4/CHCl_3$ (7/3, v/v) (blue) excited at 325 nm ($slit_{ex}$ = 8 nm, $slit_{em}$ = 12 nm). (b) Normalized excitation spectra of **2-H** (1 μM) in $CCl_4/CHCl_3$ (7/3, v/v) monitored at 385 nm (purple) and 455 nm (green) with background subtraction ($slit_{ex}$ = 8 nm, $slit_{em}$ = 12 nm).

free monomers of **2-H**. This observation suggests that macrocycle **2-H** most likely formed H-type aggregates,[21a] i.e., the macrocylic molecules stack face-to-face into tubular stacks.

The same difference in emission and exciation bands also exists in the spectra of **2-Me**, **2-F**, and **2-NH_2** (Figures S32–S34) in DMF and $CCl_4/CHCl_3$ (7/3, v/v), suggesting that all four macrocycles **2** undergo the same assembly by stacking into tubular stacks that are chiral as indicated by their circular dichroism spectra (Figure S35).

Tubular Stacking of 2 Is Confirmed by Atomic Force Microscopy (AFM). Additional evidence showing the tubular stacking of **2** is provided by AFM images (Figures 3 and S36–39), which reveal very similar fine nanofilaments. The measured distances between adjacent nanofilaments are 2.8 ± 0.2 nm for **2-H** and **2-Me**, 2.8 ± 0.3 nm for **2-F**, and 2.7 ± 0.2 nm for **2-NH_2**. These values are consistent with the diameter of the macrocycles, confirming that **2-H**, **2-Me**, **2-F**, and **2-NH_2**, with the same periphery, indeed superpose into well-aligned nanotubes.

Macrocycles 2 Show Different Behavior for Proton Transport. The tubular assemblies of **2**, consisting of macrocyclic molecules stacked directly on top of one another, should contain cylindrical pores defined by the cavities of the macrocycles. A transmembrane pore, consisting of about 10 stacked macrocyclic molecules[7,17] and thus having about 10 **X** groups on its inner surface, may exhibit mass-transport behavior that is influenced by the **X** groups.

A vesicle-based stopped-flow kinetic assay was adopted to monitor proton transport across lipid bilayers. Large unilamellar vesicles (LUVs) of the phospholipid 1-palmitoyl-2-oleoyl-*sn*-glycero-3-phosphocholine (POPC) were prepared with encapsulated 8-hydroxypyrene-1,3,6-trisulfonate (HPTS, 0.1 mM), a pH-sensitive fluorescent dye,[22] in 100 mM HEPES,

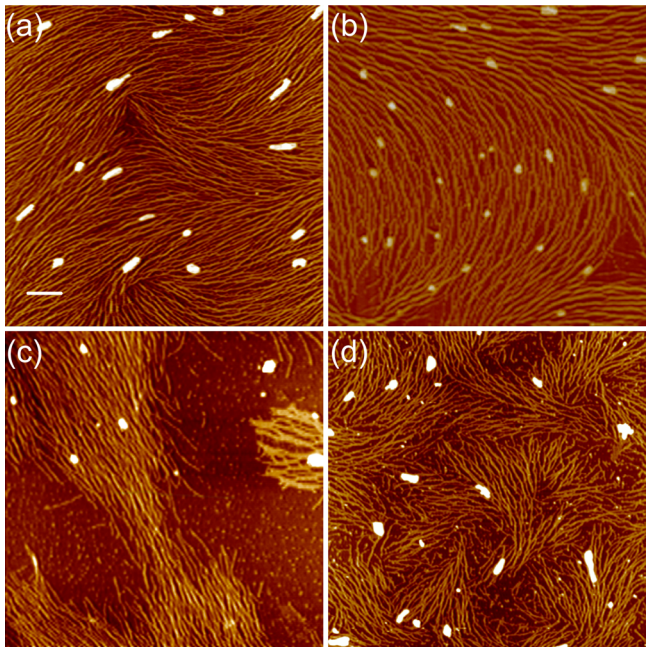

Figure 3. AFM images of **2-H** (a), **2-Me** (b), **2-F** (c), and **2-NH_2** (d). Each compound (10 μM in $CHCl_3$) was deposited on freshly cleaved mica, then incubated in saturated CCl_4 vapor overnight. AFM imaging was performed in air with the tapping mode (scale bar = 300 nm).

145 mM KCl, at pH 7.0. Each of compounds **2** was mixed with the lipid by dissolving in chloroform before the LUVs were prepared, with a molar ratio of lipid to compound of 263 to 1 and a final concentration of 10 μM in the solution used for the stopped-flow assay.

Stopped-flow kinetic assay was performed by rapidly mixing a solution (80 μL) of the LUVs with one of compounds **2** incorporated (in 100 mM HEPES, 145 mM KCl, pH 7.0) and a solution of a more acidic buffer (100 mM HEPES, 145 mM KCl, 80 mM HCl) at an equal volume in a stopped-flow spectrometer at 12 °C. The time-dependent change in the fluorescence emission of the encapsulated HPTS was monitored at 510–550 nm with the excitation wavelength being set at 450 nm. A control experiment was also performed under the same condition without incorporating any of compounds **2**. Before each fluorescence measurement, the vesicles were pre-incubated for 5 min with 5 μM of valinomycin, a potassium carrier that serves to counter the charge buildup caused by proton influx and thus retains the membrane potential to near zero, which eliminates a limiting factor in the kinetic measurements.[23]

The emission intensity of the pH-sensitive HPTS encapsulated in the LUVS serves as a direct indicator for the pH value inside the vesicles. With a higher extravesicular proton concentration, proton influx leads to an increase of acidity inside the vesicles and thus quenching of the fluorescence emission of HPTS.

As shown in Figure 4, while significant enhancement of proton transport is observed in the presence of **2-H** and **2-F**, no transport above background is detected with **2-Me** or **2-NH_2**. Results from the stopped-flow kinetic measurements provide a background proton permeability of about 2.1×10^{-9} m/s for the vesicles in the control experiment, while the proton permeability in the presence of **2-H** is 8.5×10^{-9} m/s, which is four times that of the control. The values of proton

DOI: 10.1021/jacs.5b12698
J. Am. Chem. Soc. 2016, 138, 2749–2754

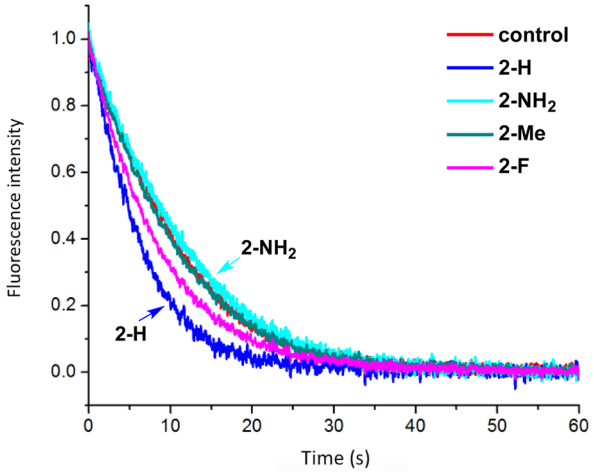

Figure 4. Results from stopped-flow measurements of the emission intensity of HPTS (0.1 mM) entrapped in 100 nm POPC LUVs in the presence of macrocycles **2** (10 μM in a pH-7.0 buffer). The LUVs were pre-incubated with valinomycin (5 μM) for 5 min and then exposed to a proton gradient by rapidly mixing with an equal volume of another solution (buffer with 80 mM HCl).

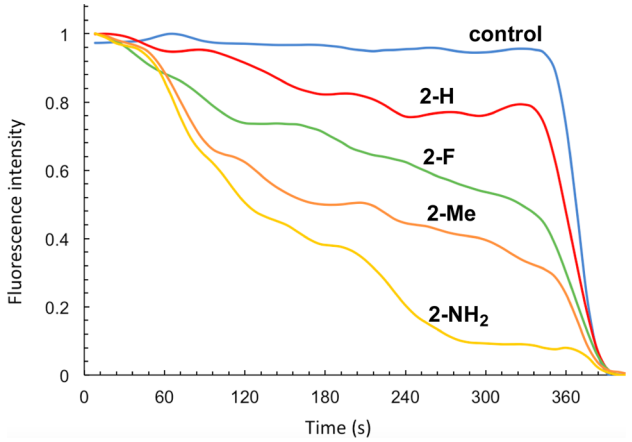

Figure 5. Normalized emission intensity of MQAE encapsulated inside POPC LUVs. Solutions of chloride-free LUVs with MQAE (10 mM) were first incubated in an isotonic buffer (pH 7.4) containing KCl (100 mM) for 1 min. Aliquots of THF and solutions (1 mM) of each of **2** in THF were added (final concentratuon of a compound = 10 μM in solution). Emission intensity at 460 nm (λ_{ex} = 354 nm) was monitored. Triton X-100 was added to rupture the LUVs.

permeability in the presence of the other three macrocycles are 2.1×10^{-9} m/s (**2-Me**), 4.6×10^{-9} m/s (**2-F**), and 2.0×10^{-9} m/s (**2-NH$_2$**), respecitvely. Thus, the presence of macrocycles **2-Me** or **2-NH$_2$** does not lead to proton transport that is higher than that of the background, while adding **2-H** or **2-F** results in proton transport that is noticeably above that of the background.

Given their identical periphery, the different behavior of **2-H**, **2-Me**, **2-F**, and **2-NH$_2$** toward proton transport can only be attributed to the membrane-spanning inner pores offered by the tubular assemblies of these macrocycles. Due to their different **X** groups, the self-assembling pores of **2** have different properties and thus behave differently when mediating transmembrane proton transport.

Macrocycles 2 Have Different Propensities for Transporting Chloride Ion. The lack of enhanced proton transport with **2-Me** or **2-NH$_2$** may be due to a simple reason: the methyl or amino groups sealed off the self-assembling pores to keep any ions from passing through. This possibility was examined with the likely transport of other ions. Rapid monitoring of chloride transport can be conveniently performed with LUVs containing *N*-(ethoxycarbonylmethyl)-6-methoxyquinolinium bromide (MQAE),[24] a chloride-sensitive dye (Figure 5). Contrary to the control experiment which did not include any of macrocycles **2** and showed little chloride transport, the presence of macrocycles **2** facilitated chloride transport to different extents. While **2-H** was found to lead to a small decrease in fluorescence emission, a significant reduction in emission intensity was observed with **2-NH$_2$**. The chloride transport activities of **2-Me** and **2-F** are between those of **2-H** and **2-NH$_2$**. Thus, the pores of **2-Me** and **2-NH$_2$**, being impermeable to proton but still conducting chloride, are not physically blocked. The differential enhancement of chloride transport in the presence of **2-NH$_2$** could be due to the numerous amino Hs in the inner pore of the tubular assembly of **2-NH$_2$**. Being placed *para* to the electron-withdrawing carbonyl group of the amide side chain and electronically similar to that of a primary amide, the NH$_2$ group of **2-NH$_2$** has Hs with a significant partial positive charge that interacts repulsively with proton but attractively with chloride ions.

Macrocycles 2-H and 2-NH$_2$ Form Single Channels with Different Cation/Anion Preferences. Conclusive evidence for the existence of transmembrane ion channels was provided by single-channel electrophysiology, which involves the measurement of electric current across a planar lipid bilayer that separates two, i.e., *cis* and *trans*, chambers, each of which holds a 1 mL saline solution. Details of preparing planar lipid bilayers can be found in the Supporting Information and in our previous reports.[7,17] Examining **2-H** and **2-NH$_2$** in 0.5 M KCl revealed long-lasting single conductance steps (Figure 6a,b) with single-channel conductance of 238 ± 60 and 231 ± 44 pS, respectively.

The cation/anion preferences of **2-H** and **2-NH$_2$** channels were compared by determining reversal potentials (ΔVs),[25] which involved creating a salt gradient and measuring currents across lipid bilayers (Supporting Information). The *x*-intercepts of the *I*/*V* plots (Figure 6c,d) reveal ΔVs of −14.09 mV and −9.68 mV for **2-H** and **2-NH$_2$**, respectively. The ΔV of **2-H** is closer to, and that of **2-NH$_2$** is much smaller than, the Nernst potential of K^+ (−17.81 mV). Calculations based on the Goldman−Hodgkin−Katz (GHK) flux equation,[25] which describes the ionic flux across a cell membrane as a function of the transmembrane potential and the concentrations of the ion inside and outside of the cell, revealed K^+/Cl^- permeability ratios (P_{K^+}/P_{Cl^-}) of 9 for the **2-H** channel and of 3.5 for the **2-NH$_2$** channel. Thus, with similar conductance, the **2-H** channel mainly transports K^+, while the **2-NH$_2$** channel shows a signficantly lowered preference for K^+, which is accompanied by enhanced Cl^- conductance.

The overall electrostatic charges of the cavities of **2** were estimated computationally (Figure 7), results from which largely reflect the observed ion transport behavior of these molecules by showing a rough correlation to the observed cation/anion transporting preferences. With cavities that are more negative than those of **2-Me** and **2-NH$_2$**, macrocycles **2-H** and **2-F** form channels that enhance proton, but not chloride transport. In contrast, the **2-Me** and **2-NH$_2$** channels exhibit the opposite trend.

The rejection of the smallest cation, i.e., H^+, but not K^+, by **2-Me** and **2-NH$_2$** is remarkable, given that proton rejection is an

DOI: 10.1021/jacs.5b12698
J. Am. Chem. Soc. 2016, 138, 2749−2754

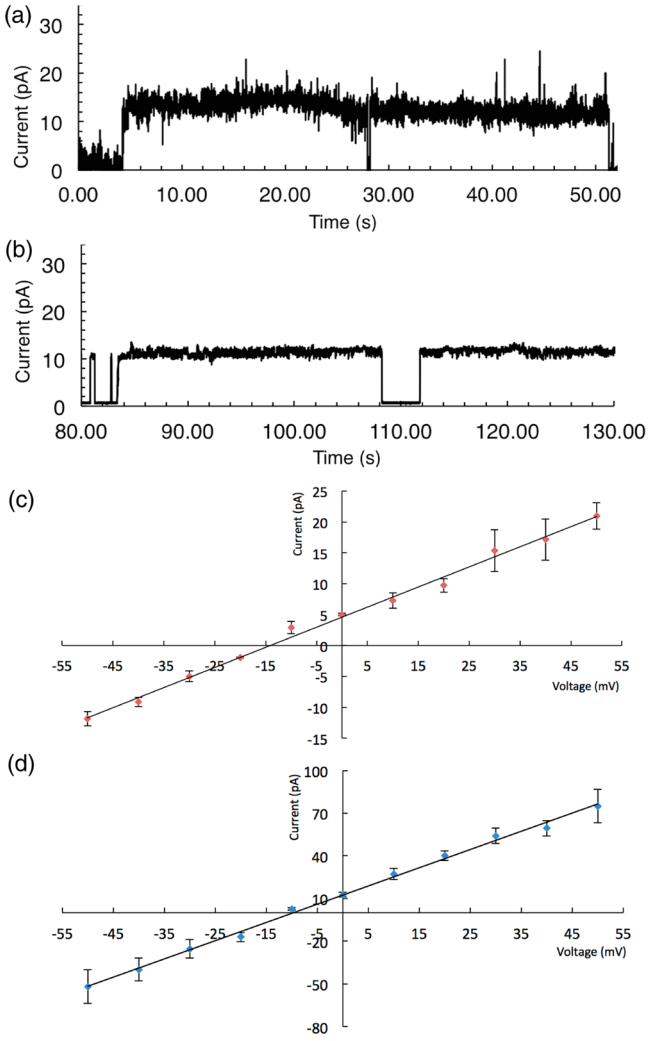

Figure 6. Single-channel recordings of (a) **2-H** and (b) **2-NH$_2$** (0.5 μM, 50 mV in 0.5 M KCl). Current–voltage plots of the channels formed by (c) **2-H** (0.5 μM) and (d) **2-NH$_2$** (0.5 μM) from reversal potential experiments (25 °C; *cis* chamber: 1 M KCl; *trans* chamber: 0.5 M KCl).

ability observed with biological channels such as aquaporins[26] but realized with few synthetic channels.[27] Whether such an effect involves the so-called orientational H-bonding defect in which structured water[28] in a nanopore is physically and/or electrostatically interrupted by methyl or amino group remains to be elucidated.

In conclusion, with a hybrid backbone and the same set of side chains, macrocycles **2** undergo the same nanotubular assembly that is demonstrated by analysis using multiple techniques. The formation of tubular assemblies with the same outer surface but different inner pores defined by stacked macrocycles **2** is also supported by the distinctly different ion-transporting behavior of these molecules. That the properties of the self-assembling pores directly influence ion transport behavior is shown by the different preferences of macrocycles **2** for transporting protons and chloride ions, due to the presence of the **X** groups. The rejection of proton by the **2-Me** and **2-NH$_2$** channels is a surprising and extraordinary capability rarely observed with synthetic channels. The different propensities of the four macrocycles **2** for transporting chloride ions point to the possibility of performing systematic structural

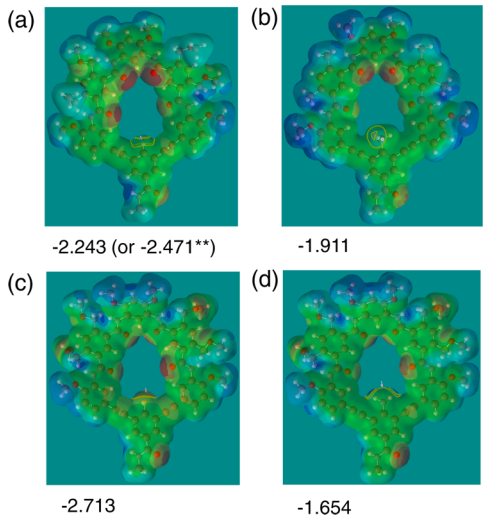

Figure 7. Electrostatic potential maps of (a) **2-H**, (b) **2-Me**, (c) **2-F**, and (d) **2-NH$_2$**. Geometry optimization and energy minimization were performed with density function B3LYP 6-31G** in vacuum. Both GAMESS and Spartan were used for the calculation of the electrostatic potential maps, along with the local ionization potential maps. The overall electrostatic charge of the inner cavity of each macrocycle, which was calculated by adding the charges of the atoms that define the cavity, is shown under each map. For **2-Me**, **2-F**, and **2-NH$_2$**, the charges of all the carbonyl oxygen atoms, along with F, or the methyl or amino Hs, are included. *Value obtained by including the charges of the two triple bonds flanking the aromatic H atom, based on the expectation that the inward-pointing H atom of **2-H**, with its small size, does not exclude the π electrons of the triple bonds from being part of the edge of the inner cavity of **2-H**.

and functional tuning of the corresponding self-assembling nanopores and the channels based on them. Understanding the mechanisms governing the observed ion transport is fundamentally important and will undoubtedly facilitate further refined design of functional nanopores, leading to a host of synthetic channels and devices with tailored selectivity and specificity.

■ ASSOCIATED CONTENT

Supporting Information

The Supporting Information is available free of charge on the ACS Publications website at DOI: 10.1021/jacs.5b12698.

Synthetic and experimental details, AFM images, NMR, mass, fluorescence and CD spectra (PDF)

■ AUTHOR INFORMATION

Corresponding Authors

*bgong@buffalo.edu
*zs9q@virginia.edu
*luzl@bnu.edu.cn

Author Contributions

‡These authors contributed equally.

Notes

The authors declare no competing financial interest.

■ ACKNOWLEDGMENTS

We thank the Natural Science Foundation of China (91227109, 11374207, 21303104, 21273148) and the US National Science Foundation (CHE-1306326 and CBET-1512124) for support.

DOI: 10.1021/jacs.5b12698
J. Am. Chem. Soc. 2016, 138, 2749–2754

REFERENCES

(1) (a) Bayley, H.; Cremer, P. S. *Nature* **2001**, *413*, 226. (b) Sakai, N.; Mareda, J.; Matile, S. *Acc. Chem. Res.* **2008**, *41*, 1354. (b) Rebek, J. *Acc. Chem. Res.* **2009**, *42*, 1660. (c) Childers, W. S.; Ni, R.; Mehta, A. K.; Lynn, D. G. *Curr. Opin. Chem. Biol.* **2009**, *13*, 652. (d) Gong, B.; Shao, Z. F. *Acc. Chem. Res.* **2013**, *46*, 2856.

(2) (a) Das, G.; Matile, S. *Proc. Natl. Acad. Sci. U. S. A.* **2002**, *99*, 5183. (b) Percec, V.; Dulcey, A. E.; Balagurusamy, V. S. K.; Miura, Y.; Smidrkal, J.; Peterca, M.; Nummelin, S.; Edlund, U.; Hudson, S. D.; Heiney, P. A.; Hu, D. A.; Magonov, S. N.; Vinogradov, S. A. *Nature* **2004**, *430*, 764. (c) Fujita, D.; Suzuki, K.; Sato, S.; Yagi-Utsumi, M.; Yamaguchi, Y.; Mizuno, N.; Kumasaka, T.; Takata, M.; Noda, M.; Uchiyama, S.; Kato, K.; Fujita, M. *Nat. Commun.* **2012**, *3*, 1093. (d) Zhang, K. D.; Ajami, D.; Gavette, J. V.; Rebek, J. *J. Am. Chem. Soc.* **2014**, *136*, 5264.

(3) (a) Bong, D. T.; Clark, T. D.; Granja, J. R.; Ghadiri, M. R. *Angew. Chem., Int. Ed.* **2001**, *40*, 988. (b) Gin, D. L.; Gu, W. Q.; Pindzola, B. A.; Zhou, W. J. *Acc. Chem. Res.* **2001**, *34*, 973. (c) Keizer, H. M.; Sijbesma, R. P. *Chem. Soc. Rev.* **2005**, *34*, 226. (d) Block, M. A. B.; Kaiser, C.; Khan, A.; Hecht, S. *Top. Curr. Chem.* **2005**, *245*, 89. (e) Pasini, D.; Ricci, M. *Curr. Org. Synth.* **2007**, *4*, 59.

(4) (a) Ghadiri, M. R.; Granja, J. R.; Milligan, R. A.; McRee, D. E.; Khazanovich, N. *Nature* **1993**, *366*, 324. (b) Seebach, D.; Matthews, J. L.; Meden, A.; Wessels, T.; Baerlocher, C.; McCusker, L. B. *Helv. Chim. Acta* **1997**, *80*, 173. (c) Gattuso, G.; Menzer, S.; Nepogodiev, S. A.; Stoddart, J. F.; Williams, D. J. *Angew. Chem., Int. Ed. Engl.* **1997**, *36*, 1451. (d) Mindyuk, O. Y.; Stetzer, M. R.; Heiney, P. A.; Nelson, J. C.; Moore, J. S. *Adv. Mater.* **1998**, *10*, 1363. (e) Fritzsche, M.; Bohle, A.; Dudenko, D.; Baumeister, U.; Sebastiani, D.; Richardt, G.; Spiess, H. W.; Hansen, M. R.; Höger, S. *Angew. Chem., Int. Ed.* **2011**, *50*, 3030. (f) Frischmann, P. D.; Sahli, B. J.; Guieu, S.; Patrick, B. O.; MacLachlan, M. J. *Chem. - Eur. J.* **2012**, *18*, 13712. (g) Hjelmgaard, T.; Roy, O.; Nauton, L.; El-Ghozzi, M.; Avignant, D.; Didierjean, C.; Taillefumier, C.; Faure, S. *Chem. Commun.* **2014**, *50*, 3564. (h) Zhao, H. Q.; Sheng, S.; Hong, Y. H.; Zeng, H. Q. *J. Am. Chem. Soc.* **2014**, *136*, 14270.

(5) Alexiadis, A.; Kassinos, S. *Chem. Rev.* **2008**, *108*, 5014.

(6) (a) Hummer, G.; Rasaiah, J. C.; Noworyta, J. P. *Nature* **2001**, *414*, 188. (b) Holt, J. K.; Park, H. G.; Wang, Y. M.; Stadermann, M.; Artyukhin, A. B.; Grigoropoulos, C. P.; Noy, A.; Bakajin, O. *Science* **2006**, *312*, 1034. (c) Lee, C. Y.; Choi, W. J.; Han, J. H.; Strano, M. S. *Science* **2010**, *329*, 1320.

(7) Zhou, X. B.; Liu, G. D.; Yamato, K.; Shen, Y.; Cheng, R. X.; Wei, X. X.; Bai, W. L.; Gao, Y.; Li, H.; Liu, Y.; Liu, F. T.; Czajkowsky, D. M.; Wang, J. F.; Dabney, M. J.; Cai, Z. H.; Hu, J.; Bright, F. V.; He, L.; Zeng, X. C.; Shao, Z. F.; Gong, B. *Nat. Commun.* **2012**, *3*, 949.

(8) (a) Yuan, L. H.; Feng, W.; Yamato, K.; Sanford, A. R.; Xu, D. G.; Guo, H.; Gong, B. *J. Am. Chem. Soc.* **2004**, *126*, 11120. (b) Feng, W.; Yamato, K.; Yang, L. Q.; Ferguson, J.; Zhong, L. J.; Zou, S. L.; Yuan, L. H.; Zeng, X. C.; Gong, B. *J. Am. Chem. Soc.* **2009**, *131*, 2629.

(9) (a) Yamato, K.; Kline, M.; Gong, B. *Chem. Commun.* **2012**, *48*, 12142. (b) He, L.; An, Y.; Yuan, L. H.; Feng, W.; Li, M. F.; Zhang, D. C.; Yamato, K.; Zheng, C.; Zeng, X. C.; Gong, B. *Proc. Natl. Acad. Sci. U. S. A.* **2006**, *103*, 10850. (c) Ferguson, J. S.; Yamato, K.; Liu, R.; He, L.; Zeng, X. C.; Gong, B. *Angew. Chem., Int. Ed.* **2009**, *48*, 3150.

(10) (a) Moore, J. S.; Zhang, J. *Angew. Chem., Int. Ed. Engl.* **1992**, *31*, 922. (b) Höger, S.; Enkelmann, V. *Angew. Chem., Int. Ed. Engl.* **1995**, *34*, 2713. (c) Hensel, V.; Lutzow, K.; Schlüter, A.-D.; Jacob, J.; Gessler, K.; Saenger, W. *Angew. Chem., Int. Ed. Engl.* **1997**, *36*, 2654.

(11) (a) Jiang, H.; Léger, J.-M.; Guionneau, P.; Huc, I. *Org. Lett.* **2004**, *6*, 2985. (b) Campbell, F.; Plante, J.; Carruthers, C.; Hardie, M. J.; Prior, T. J.; Wilson, A. J. *Chem. Commun.* **2007**, 2240. (c) Qin, B.; Ren, C.; Ye, R.; Sun, C.; Chiad, K.; Chen, X.; Li, Z.; Xue, F.; Su, H.; Chass, G. A.; Zeng, H. Q. *J. Am. Chem. Soc.* **2010**, *132*, 9564.

(12) (a) Xing, L.; Ziener, U.; Sutherland, T. C.; Cuccia, L. A. *Chem. Commun.* **2005**, 5751. (b) Gube, A.; Komber, H.; Sahre, K.; Friedel, P.; Voit, B.; Böhme, F. *J. Org. Chem.* **2012**, *77*, 9620.

(13) (a) Sessler, J. L.; Tomat, E.; Lynch, V. M. *Chem. Commun.* **2006**, 4486. (b) Holub, J. M.; Jang, H. J.; Kirshenbaum, K. *Org. Lett.* **2007**, *9*, 3275. (c) Frischmann, P. D.; Facey, G. A.; Ghi, P. Y.; Gallant, A. J.; Bryce, D. L.; Lelj, F.; MacLachlan, M. J. *J. Am. Chem. Soc.* **2010**, *132*, 3893. (d) Lee, S.; Chen, C.-H.; Flood, A. H. *Nat. Chem.* **2013**, *5*, 704. (e) Fu, H. L.; Liu, Y.; Zeng, H. Q. *Chem. Commun.* **2013**, *49*, 4127.

(14) Yang, Y. A.; Feng, W.; Hu, J. C.; Zou, S. L.; Gao, R. Z.; Yamato, K.; Kline, M.; Cai, Z. H.; Gao, Y.; Wang, Y. B.; Li, Y. B.; Yang, Y. L.; Yuan, L. H.; Zeng, X. C.; Gong, B. *J. Am. Chem. Soc.* **2011**, *133*, 18590.

(15) (a) Wu, X. X.; Liang, G. X.; Ji, G.; Fun, H. K.; He, L.; Gong, B. *Chem. Commun.* **2012**, *48*, 2228. (b) Wu, X. X.; Rui Liu, R.; Sathyamoorthy, B.; Yamato, K.; Liang, G. X.; Shen, L.; Ma, S. F.; Sukumaran, D. K.; Szyperski, T.; Fang, W. H.; He, L.; Chen, X. B.; Gong, B. *J. Am. Chem. Soc.* **2015**, *137*, 5879.

(16) (a) Kline, M.; Wei, X. X.; Gong, B. *Org. Lett.* **2013**, *15*, 4762. (b) Kline, M. A.; Wei, X. X.; Horner, I. J.; Liu, R.; Chen, S.; Chen, S.; Yung, K. Y.; Yamato, K.; Cai, Z. H.; Bright, F. V.; Zeng, X. C.; Gong, B. *Chem. Sci.* **2015**, *6*, 152.

(17) Helsel, A. J.; Brown, A. L.; Yamato, K.; Feng, W.; Yuan, L. H.; Clements, A.; Harding, S. V.; Szabo, G.; Shao, Z. F.; Gong, B. *J. Am. Chem. Soc.* **2008**, *130*, 15784.

(18) (a) Sakai, N.; Matile, S. *Langmuir* **2013**, *29*, 9031. (b) Zhao, Y.; Cho, H. K.; Widanapathirana, L.; Zhang, S. Y. *Acc. Chem. Res.* **2013**, *46*, 2763. (c) Gokel, G. W.; Negin, S. *Acc. Chem. Res.* **2013**, *46*, 2824. (d) Fyles, T. *Acc. Chem. Res.* **2013**, *46*, 2847. (e) Otis, F.; Auger, M.; Voyer, N. *Acc. Chem. Res.* **2013**, *46*, 2934. (f) Montenegro, J.; Ghadiri, M. R.; Granja, J. R. *Acc. Chem. Res.* **2013**, *46*, 2955. (g) Mayer, M.; Yang, J. *Acc. Chem. Res.* **2013**, *46*, 2998. (h) Chui, J. K. W.; Fyles, T. M. *Chem. Soc. Rev.* **2012**, *41*, 148. (i) Davis, J. T.; Okunola, O.; Quesada, R. *Chem. Soc. Rev.* **2010**, *39*, 3843.

(19) (a) Parra, R. D.; Furukawa, M.; Gong, B.; Zeng, X. C. *J. Chem. Phys.* **2001**, *115*, 6030. (b) Parra, R. D.; Gong, B.; Zeng, X. C. *J. Chem. Phys.* **2001**, *115*, 6036.

(20) Yang, L. Q.; Zhong, L. J.; Yamato, K.; Zhang, X. H.; Feng, W.; Deng, P. C.; Yuan, L. H.; Zeng, X. C.; Gong, B. *New J. Chem.* **2009**, *33*, 729.

(21) (a) Birk, J. B. *Photophysics of Aromatic Molecules*. Wiley-Interscience: New York, 1970. (b) Prince, R. B.; Saven, J. G.; Wolynes, P. G.; Moore, J. S. *J. Am. Chem. Soc.* **1999**, *121*, 3114.

(22) Clement, N. R.; Gould, J. M. *Biochemistry* **1981**, *20*, 1534.

(23) (a) Nichols, J. W.; Deamer, D. W. *Proc. Natl. Acad. Sci. U. S. A.* **1980**, *77*, 2038. (b) Weiss, L. A.; Sakai, N.; Ghebremariam, B.; Ni, C.; Matile, S. *J. Am. Chem. Soc.* **1997**, *119*, 12142.

(24) Verkman, A. S. *Am. J. Physiol.* **1990**, *259*, C375.

(25) Hille, B. *Ionic Channels of Excitable Membranes*, 3rd ed.; Sinauer: Sunderland, MA, 2001.

(26) de Groot, B. L.; Frigato, T.; Helms, V.; Grubmuller, H. *J. Mol. Biol.* **2003**, *333*, 279.

(27) Hu, X. B.; Chen, Z.; Tang, G.; Hou, J. L.; Li, Z. T. *J. Am. Chem. Soc.* **2012**, *134*, 8384.

(28) (a) Cao, Z.; Peng, Y. X.; Yan, T. Y.; Li, S.; Li, A. L.; Voth, G. A. *J. Am. Chem. Soc.* **2010**, *132*, 11395. (b) Dellago, C.; Naor, M. M.; Hummer, G. *Phys. Rev. Lett.* **2003**, *90*, 105902.

DOI: 10.1021/jacs.5b12698
J. Am. Chem. Soc. 2016, 138, 2749−2754